ICE SHEETS

Deglaciation of northwestern Greenland during Marine Isotope Stage 11

Andrew J. Christ[1,2]*, Tammy M. Rittenour[3], Paul R. Bierman[1,2]*, Benjamin A. Keisling[4], Paul C. Knutz[5], Tonny B. Thomsen[5], Nynke Keulen[5], Julie C. Fosdick[6], Sidney R. Hemming[7], Jean-Louis Tison[8], Pierre-Henri Blard[8,9], Jørgen P. Steffensen[10], Marc W. Caffee[11,12], Lee B. Corbett[2], Dorthe Dahl-Jensen[10,13], David P. Dethier[14], Alan J. Hidy[15], Nicolas Perdrial[1,16], Dorothy M. Peteet[7,17], Eric J. Steig[18], Elizabeth K. Thomas[19]

Past interglacial climates with smaller ice sheets offer analogs for ice sheet response to future warming and contributions to sea level rise; however, well-dated geologic records from formerly ice-free areas are rare. Here we report that subglacial sediment from the Camp Century ice core preserves direct evidence that northwestern Greenland was ice free during the Marine Isotope Stage (MIS) 11 interglacial. Luminescence dating shows that sediment just beneath the ice sheet was deposited by flowing water in an ice-free environment 416 ± 38 thousand years ago. Provenance analyses and cosmogenic nuclide data and calculations suggest the sediment was reworked from local materials and exposed at the surface <16 thousand years before deposition. Ice sheet modeling indicates that ice-free conditions at Camp Century require at least 1.4 meters of sea level equivalent contribution from the Greenland Ice Sheet.

Global oxygen isotopic composition of seawater ($\delta^{18}O_{seawater}$) data (*1*) highlight several interglacial periods since ~1 million years ago (Ma) with global ice volume lower than present, implying that the Greenland Ice Sheet (GrIS) and/or the Antarctic Ice Sheet were previously smaller than today. The lowest global ice volumes occurred during Marine Isotope Stage (MIS) 31 (1.08 to 1.06 Ma) and MIS 11 [424 to 374 thousand years ago (ka)]. Moderately lower ice volumes occurred during MIS 9 (337 to 300 ka), and MIS 5 (130 to 71 ka). Global mean sea level (GMSL) reconstructions indicate that the interglacials with the highest sea level were MIS 11 (+6 to 13 m) (*2*, *3*) and MIS 5 (+1.2 to 5.3 m) (*4*), consistent with substantial reduction of the GrIS. However, the configuration of the GrIS, and thus its contribution to GMSL, during past interglacial periods remains poorly constrained (*3*).

Marine sediment archives document fluctuations in GrIS extent since ~1 Ma. Ice-rafted debris (IRD) in marine sediment from the North Atlantic Ocean indicates variable but persistent marine-terminating glaciation in eastern Greenland (Fig. 1) (*5*). Increased ^{10}Be concentrations in IRD during some intervals can be interpreted as a record of glacial erosion of landscapes exposed by smaller GrIS configurations during the Pleistocene (*6*). In the Labrador Sea, provenance changes in silt-sized sediment suggest that the southern GrIS retreated slightly during MIS 9 and 5 and was almost entirely absent during MIS 11 (*7*–*9*). Pollen in Labrador Sea sediment indicates that southern Greenland was inhabited by boreal forests during MIS 11 and possibly MIS 13 (533 to 478 ka), by tundra during MIS 7 (243 to 191 ka), and by fern-dominated (Pteridophyta) ecosystems during MIS 5 and perhaps MIS 9 (*10*). Compared to the Holocene, sea surface temperatures in the Labrador Sea were much warmer during MIS 9, 7, and 5 for brief periods [12.2, 4.4, and 9.7 thousand years (kyr), respectively] and slightly warmer during MIS 11 for a longer duration (20.7 kyr) (*11*, *12*). Terrestrial temperatures reconstructed from leaf-wax biomarkers show that several interglacials since 600 ka were warmer than the Holocene, including brief extreme warmth during MIS 5 and prolonged moderate warmth during MIS 11 (*13*) (Fig. 1B).

Age constraints of Greenland ice core b… materials require substantial GrIS retrea… least once since ~1 Ma (Fig. 1B). Silty ice from the bottom of the Greenland Ice Core Project (GRIP) ice core suggests glacial cover in central Greenland since 950 ± 44 ka ($^{10}Be/^{36}Cl$) (*14*) and 970 ± 140 ka ($\delta^{40}Ar/^{38}Ar$) (*15*). Nearby, at the Greenland Ice Sheet Project 2 (GISP2) ice core, basal ice has $\delta^{40}Ar/^{38}Ar$ ages of >250 ka (*16*). Cosmogenic $^{26}Al/^{10}Be$ data from the underlying subglacial bedrock at GISP2 requires at least one episode of exposure, and thus ice-free conditions, in central Greenland after 1.1 ± 0.1 Ma (*17*). In southern Greenland, basal silty ice from the Dye-3 ice core contains DNA from boreal forest that occupied the area sometime between 400 and 800 ka (*14*). In the North Greenland Eemian Ice Drilling (NEEM) ice core, folded ice near the bottom of the ice core dates to MIS 5e (*18*), but the basal silty ice and underlying sediment have not been dated (*19*). In northwestern Greenland, subglacial sediment from the Camp Century ice core contains evidence for at least two ice-free events, one in the Early Pleistocene and another after 1 Ma (*20*).

The Camp Century subglacial sediment (3.44-m-long, 0.1-m-diameter core) was recovered in 1966 CE at the base of the ice core (1387 m depth) (*21*) and has yet to be extensively studied. The frozen sediment (Fig. 2A) contains an upper unit of bedded sand (0 to 0.82 m below the ice–sediment interface) unconformably overlying ice-rich graded mud, sand, and pebbles (0.82 to 1.12 m), an intermediate unit of vertically fractured sediment-laden ice (1.12 to 2.05 m), and a lower unit of diamicton containing subhorizontal ice lenses (2.05 to 3.44 m). An early investigation (*22*) that reported abundant freshwater diatoms and rare (likely windblown) marine diatoms in the Camp Century basal ice and subglacial sediment suggested that northwest Greenland was ice free and the GrIS retreated at some point during the Pleistocene. Recent analyses focused on the uppermost and lowermost samples [sample 1059-4: 0 to 0.10 m (Fig. 2B); and sample 1063-7: 3.27 to 3.40 m (Fig. 2C)] (*20*). Enriched $\delta^{18}O$ values of pore ice from these samples suggest that precipitation fell at lower elevations and/or under warmer conditions, indicating local absence of the GrIS (*20*). Plant macrofossils and sedimentary leaf-wax biomarkers provide direct evidence for a tundra ecosystem during ice-free events (*20*). Clay mineralogy and major ions from pore ice suggest that the upper and lower sediment samples have different weathering histories (*20*). $^{26}Al/^{10}Be$ data from the upper sediment require ice-free exposure at some time after 1.0 ± 0.1 Ma; however, the precise timing of this ice-free event was not constrained (*20*). The lower sediment was buried at some point between the Early Pleistocene (>1.4 Ma; infrared stimulated

[1]Rubenstein School of the Environment and Natural Resources, University of Vermont, Burlington, VT 05405, USA. [2]Gund Institute for Environment, University of Vermont, Burlington, VT 05405, USA. [3]Department of Geosciences, Utah State University, Logan, UT 84322, USA. [4]University of Texas Institute for Geophysics, Jackson School of Geosciences, University of Texas at Austin, Austin, TX 78754, USA. [5]Geological Survey of Denmark and Greenland, 1350 Copenhagen, Denmark. [6]Department of Earth Sciences, University of Connecticut, Storrs, CT 06269, USA. [7]Lamont-Doherty Earth Observatory, Columbia University, Palisades, NY 10964, USA. [8]Laboratoire de Glaciologie, DGES-IGEOS, Université Libre de Bruxelles, 1050 Brussels, Belgium. [9]Centre de Recherches Pétrographiques et Géochimiques, CNRS, Université de Lorraine, 54500 Nancy, France. [10]Centre for Ice and Climate, PICE, Niels Bohr Institute, University of Copenhagen, 2200 Copenhagen, Denmark. [11]Department of Physics and Astronomy, Purdue University, West Lafayette, IN 47907, USA. [12]Department of Earth, Atmospheric, and Planetary Sciences, Purdue University, West Lafayette, IN 47907, USA. [13]Centre for Earth Observation Science, University of Manitoba, Winnipeg, MB R3T 2N2, Canada. [14]Department of Geosciences, Williams College, Williamstown, MA 01267, USA. [15]Center for Accelerator Mass Spectrometry, Lawrence Livermore National Laboratory, Livermore, CA 94550, USA. [16]Department of Geography and Geosciences, University of Vermont, Burlington, VT 05405, USA. [17]NASA Goddard Institute for Space Studies, New York, NY 10025, USA. [18]Department of Earth and Space Sciences, University of Washington, Seattle, WA 98195, USA. [19]Department of Geology, University at Buffalo, Buffalo, NY 14260, USA.
*Corresponding author. Email: andrew.j.christ@gmail.com (A.J.C.); pbierman@uvm.edu (P.R.B.)

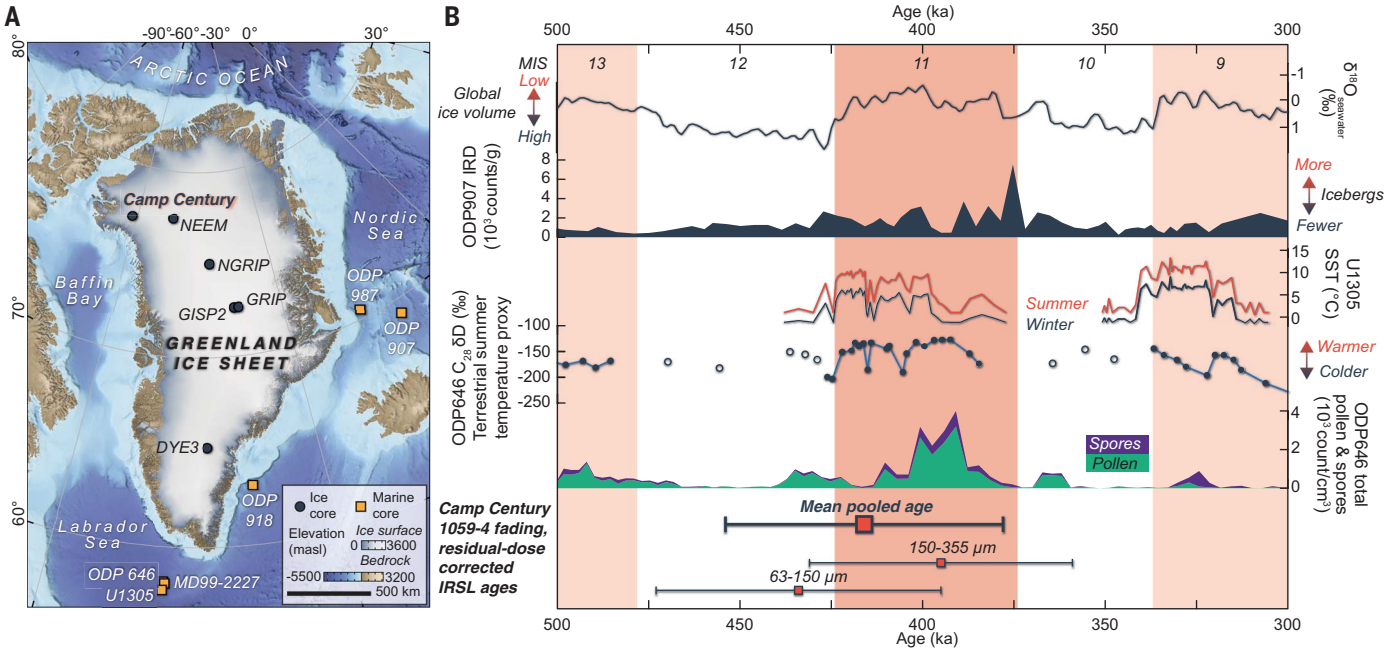

Fig. 1. Overview map and paleoclimate. (**A**) Overview map of Greenland showing marine sediment cores and ice core locations, including Camp Century. Elevation data from (*32*). masl, meters above sea level. (**B**) Paleoclimate from 500 to 300 ka: Marine Isotope Stages (MIS), with light-pink shading corresponding to interglacial periods and darker-pink shading highlighting MIS 11; $\delta^{18}O_{seawater}$, a proxy for global ice volume (*1*); Nordic Sea IRD flux (ODP 907) (*5*); southern Greenland sea surface temperature (SST; IODP U1305) (*11*); leaf-wax biomarker proxy (solid blue circles and light blue lines) for terrestrial summer temperature (ODP 646) (*13*); total counts of pollen (green) and spermatophyte spores of pteridophytes (purple) in Labrador Sea sediment (ODP 646) (*10*); and Camp Century upper sediment (1059-4) fading and residual-dose–corrected pIRSL ages (weighted mean ± 1 SE; larger red square with thick blue line shows the mean pooled age, and the smaller red squares with thin blue lines show the mean ages for each grain-size fraction).

luminescence) and Late Pliocene (<3.2 ± 0.4 Ma; $^{26}Al/^{10}Be$) (*20*).

Here, we present data that provide direct terrestrial evidence of ice sheet absence in northwestern Greenland during the MIS 11 interglacial period. We present new luminescence dates of the upper subglacial sediment (1059-4) at the base of the Camp Century ice core. When combined with in situ cosmogenic ^{26}Al and ^{10}Be measurements from the same sediment (*20*), the luminescence data allow us to constrain the timing of ice-free conditions and to model the maximum possible duration of surface exposure of the sediment. We use mineralogical and detrital geochronometric analyses (apatite U-Th/He; hornblende $^{40}Ar/^{39}Ar$; and zircon, apatite, and rutile U-Pb) to characterize the provenance of the upper (1059-4) and lower (1063-7) subglacial sediment. We use an ensemble of ice sheet models to simulate GrIS configurations that produce ice-free conditions at Camp Century and quantify the resulting sea level equivalent (SLE) contributions from the GrIS [see supplementary materials (SM) for complete explanations of materials and methods].

Sediment deposition and paleo-exposure history

Luminescence dating shows that the upper subglacial sediment from Camp Century was last exposed to sunlight 416 ± 38 ka (mean age ± 1σ) during the MIS 11 interglacial period. We dated two sand-sized fractions of potassium feldspar recovered from an interior portion of sample 1059-4 cut in darkroom conditions while frozen (Fig. 2B; SM methods). Feldspar separates were dated using post-infrared infrared-stimulated luminescence at 250°C following multiple elevated temperatures (MET pIR $IRSL_{250}$) (*23*) (SM methods; Fig. 3, figs. S1 to S4, and data S1 to S11). Anomalous fading (athermal loss of signal over time), which is common in feldspar, was corrected independently for each aliquot and pIR IRSL temperature (*24*) (SM methods; data S3 to S5). Different grain sizes from the same subsample produced fading-corrected pIR-$IRSL_{250}$ apparent ages of 459 ± 34 ka (63 to 150 μm; n = 22 aliquots; weighted mean ± 1 SE) and 416 ± 32 ka (150 to 355 μm; n = 20 aliquots) (data S1 and S4). The elevated temperature pretreatments applied in the MET pIR IRSL can subsample residual signals not reset by light, necessitating correction for their removal (SM methods; data S8) (*25*). The fading and residual-dose–corrected ages are 434 ± 39 ka (63 to 150 μm; n = 22 aliquots) and 395 ± 36 ka (150 to 355 μm; n = 20 aliquots) (Fig. 3 and data S1). Combining data from both grain-size fractions, the mean fading and residual-dose–corrected IRSL age indicates that the upper subglacial sediment was last exposed to sunlight at 416 ± 38 ka, during the MIS 11 interglacial (424 to 374 ka) (Fig. 1B and data S1). The IRSL ages record the deposition of the upper sediment after exposure to light in an ice-free environment. The coherent luminescence measurements in multiple aliquots (n = 42 total) from two grain sizes demonstrate that the IRSL age is robust and is not the result of mixing exposed and unexposed grains in sample aliquots. Notably, the absence of young ages indicates that the core interior was not exposed to light during drilling (1966 CE), sample storage (1966 to 2020 CE), or subsampling and processing (2020 CE).

The newly determined luminescence age allows us to decay-correct the measured $^{26}Al/^{10}Be$ ratio (4.4 ± 0.5) in quartz of the upper sediment (*20*) to the ratio at the time of deposition. We can then model how long the sediment was exposed at the surface before deposition. If we assume that the upper sediment was exposed at the surface, deposited, and buried since 416 ± 38 ka, then the $^{26}Al/^{10}Be$ ratio would have been 5.4 ± 0.7 at burial (Fig. 4 and fig. S5). Our model indicates that all plausible solutions require exposure durations of ≤16 kyr [assuming a Greenland-specific $^{26}Al/^{10}Be$ surface production ratio of 7.3 (*26*); SM methods]. This maximum 16 kyr exposure duration assumes irradiation at the surface; if

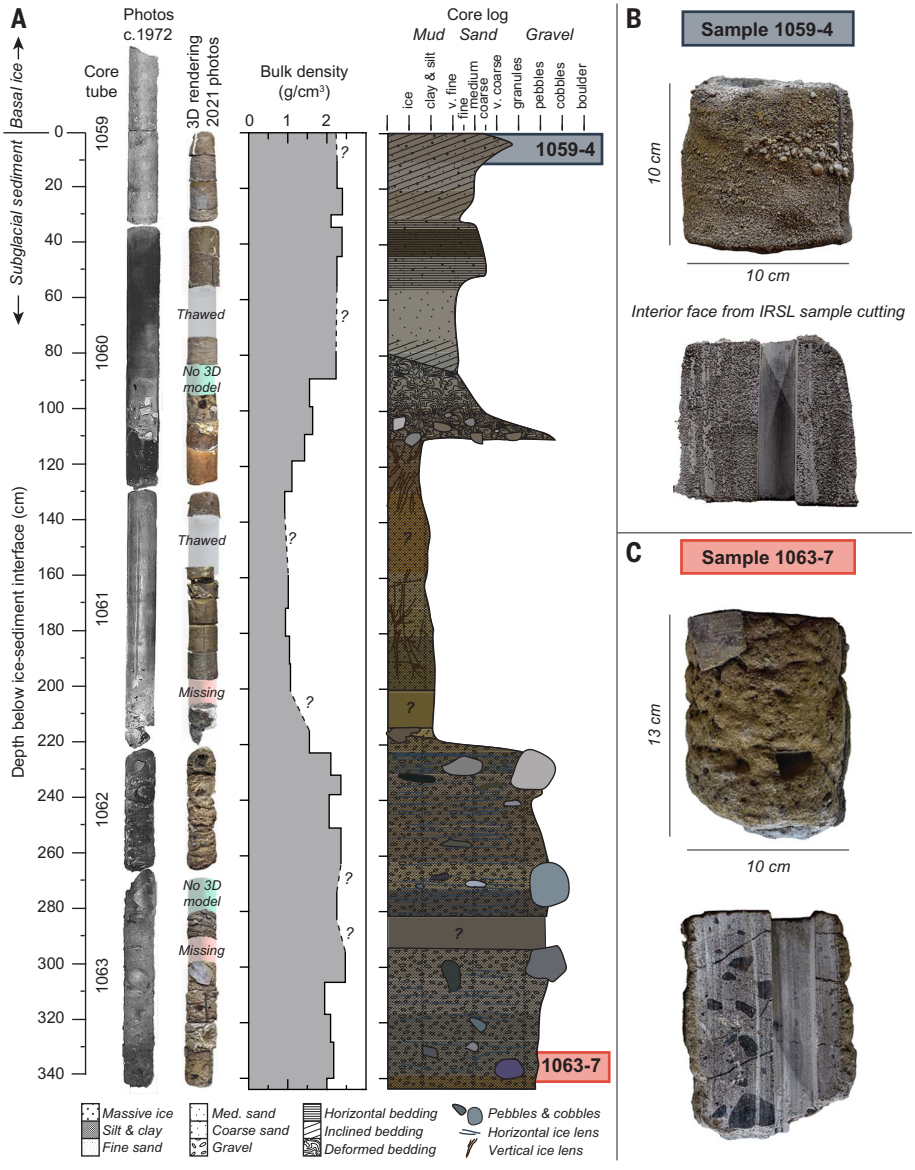

Fig. 2. Camp Century subglacial sediment core log and sample photos (**A**) Camp Century subglacial sediment original core tube photos adapted from (*44*), photogrammetric three-dimensional (3D) model renderings from recent photographs, bulk density measurements, and core log updated from (*20*) with the locations of samples 1059-4 (bluish gray) and 1063-7 (reddish pink) highlighted. Sediment core segment photographs of samples (**B**) 1059-4 and (**C**) 1063-7, showing interior and exterior core faces and the location of the luminescence sample.

nuclide production occurred at depth, then a greater maximum duration of exposure is possible.

The luminescence age–informed $^{26}Al/^{10}Be$ burial history of the upper sediment is consistent with the $^{26}Al/^{10}Be$ burial history of the underlying lower Camp Century subglacial sediment (sample 1063-7). Previous IRSL analysis of the lower sediment indicates that it was deposited >1.4 Ma (*20*), and the measured $^{26}Al/^{10}Be$ ratio (1.7 ± 0.4) suggests that the lower sediment remained buried and was shielded from substantial nuclide production while the upper sediment was exposed to cosmic rays and light during MIS 11. The $^{26}Al/^{10}Be$ ratio of the lower sediment, decay-corrected for 432 kyr of burial (416 kyr luminescence age plus a maximum of 16 kyr surface exposure), is 2.1 ± 1.2 (Fig. 4A and fig. S5). If the inherited $^{26}Al/^{10}Be$ ratio (i.e., before MIS 11 exposure) of the upper sediment was equivalent to that of the lower sample (2.1 ± 1.2), then the surface-exposure duration of the upper sediment could be no more than 14 kyr (Fig. 4A and fig. S5; SM methods). This similarity suggests that the upper sediment was sourced from material with an integrated exposure and burial history comparable to that of the lower sediment (Fig. 4B), which is consistent with the provenance data.

Sediment provenance

The upper and lower subglacial sediment samples at Camp Century have statistically indistinguishable provenance. Each of the detrital geochronometry measurements, including apatite (U-Th)/He dates, hornblende $^{40}Ar/^{39}Ar$ dates, and zircon and apatite concordant U-Pb dates (Fig. 5, figs. S6 to S8, and data S12 to S15) are similar and likely drawn from the same parent population, as shown by multiple statistical tests, including Kolmogorov-Smirnov, Kuiper, likeness, similarity, and cross-correlation coefficient (*27*) (data S16). Rutile U-Pb dates could only be determined for sample 1059-4 (fig. S8 and data S17), but those data support an 1800 to 2000 Ma probability mode in the zircon U-Pb data reflecting a Paleoproterozoic metamorphic imprint on Greenland Archaean crust (*28*, *29*). Likewise, the bulk mineralogy of the upper and lower sediment samples is similar and dominated by quartz and feldspar (Fig. 5E and data S18). The heavy mineral composition is mostly mafic silicates (amphiboles and pyroxene) and garnet, with lesser amounts of chlorite, iron oxides, apatite, and ilmenite (Fig. 5F). A Kolmogorov-Smirnov test demonstrates that the mineralogy of the upper and lower sediment is statistically similar across multiple grain sizes and mineral fractions (data S19). However, the dominance of garnet over amphibole and pyroxene [g/(A+P)] in the upper sample (0.13) compared with the lower sample (0.04) may suggest more-intense weathering of heavy minerals in the upper sediment (Fig. 5F). These observations indicate that the upper sediment formed by reworking of local materials similar to the lower sediment, consistent with our modeling of the $^{26}Al/^{10}Be$ ratio and luminescence data.

Ice sheet modeling

We used an ensemble of numerical ice sheet simulations to determine the minimum SLE contribution of the Greenland Ice Sheet required for Camp Century to be ice free (SM methods). The ensemble includes 96 different simulations varying the following parameters: rate of interglacial climate warming (1°, 1.33°, 1.66°, and 2°C/kyr), starting ice sheet configuration [Last Glacial Maximum (LGM), modern with spin-up, modern with "cold" start], starting climatology (modern or Holocene Thermal Maximum), precipitation lapse rate, and asthenosphere relaxation time. These parameters were chosen to incorporate unknowns in the interglacial MIS 11 climate and the glacial MIS 12 extent of the ice sheet to encompass a range of possible interglacial climate warming scenarios. Rates of interglacial warming were chosen to reflect the range of atmospheric warming in proxy records from around Greenland

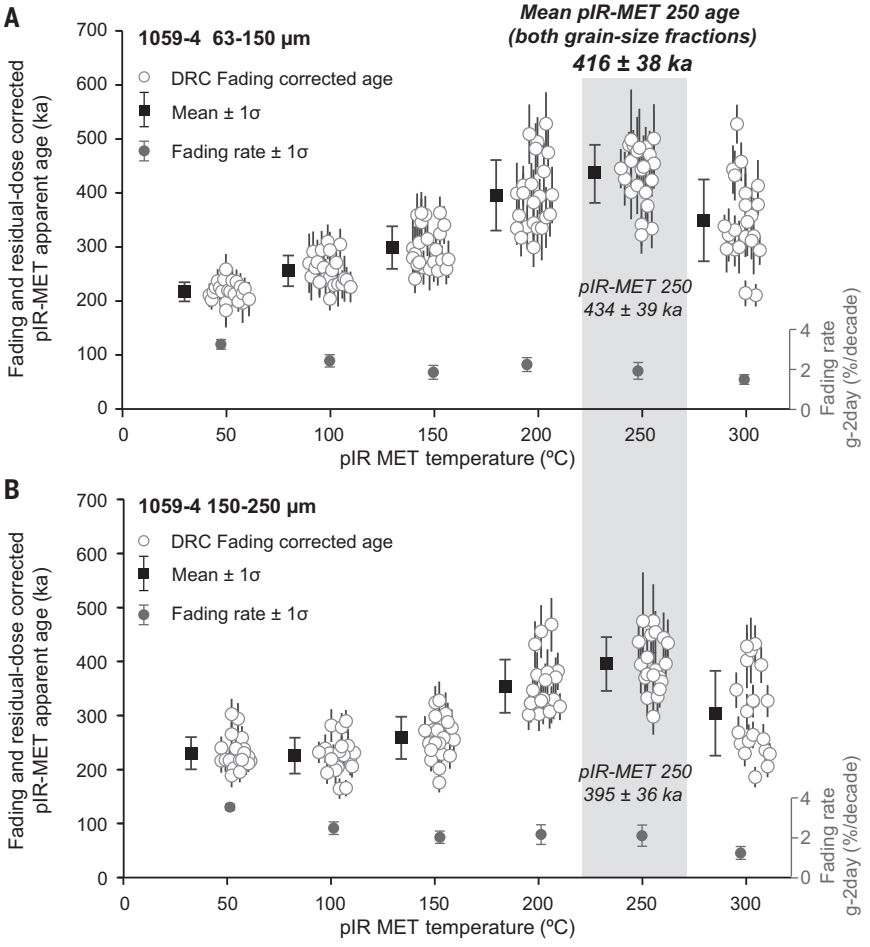

Fig. 3. Luminescence ages of the upper sediment (1059-4). Dose-response curve (DRC) faded post-infrared analysis at multiple elevated temperatures (pIR-MET IRSL) and measured fading rates in potassium feldspar aliquots from the upper sediment (1059-4) in two different grain sizes: (**A**) 63 to 150 µm and (**B**) 150 to 250 µm. Reported age and gray shading show the results for the 250°C temperature step (pIR-MET 250) used for dating.

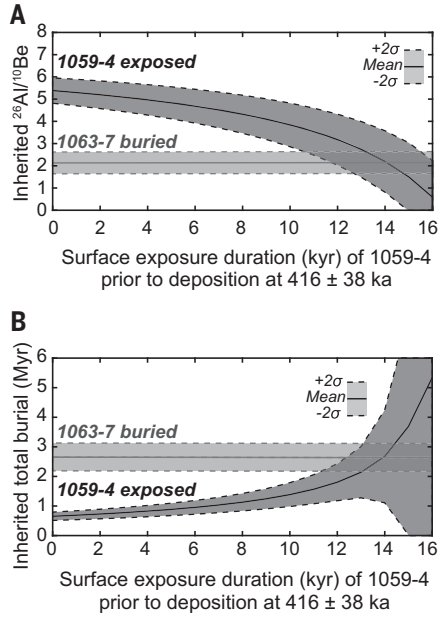

Fig. 4. Luminescence age–informed modeling of ^{26}Al/^{10}Be burial history for the upper (1059-4) and lower (1063-7) sediments. (**A**) Inherited ^{26}Al/^{10}Be ratios and (**B**) corresponding inherited total burial histories of the upper and lower sediments, given a range of surface exposure duration of the upper sediment before deposition at 416 ± 38 ka, while the lower sediment remained buried during MIS 11.

(*30*, *31*). For the analysis, we focus on the first time step in each simulation when the Camp Century site is ice free. We compiled the ice sheet extents of all simulations that produced ice-free conditions at Camp Century and the associated SLE contribution relative to the present ice sheet (*32*) (SM methods; Fig. 6A and fig. S9).

The simulation with the least amount of ice loss needed to drive deglaciation at Camp Century equates to +1.4 m of SLE contribution from the GrIS. Out of 96 hypothetical interglacials, spanning a range of uncertainties in climatological, glaciological, and solid-Earth parameters, 79 result in deglaciation at Camp Century (Fig. 6A and fig. S8; SM methods). The ice sheet geometries corresponding to the first ice-free conditions at Camp Century equate to a range of sea level contributions (1.4 to 5.5 m SLE). The simulations that provide the low-end constraint (+1.4 m SLE) start with a modern ice sheet geometry and climate and use a 2% per °C precipitation correction (Fig. 6, B and C). Starting with a glacial ice sheet configuration, using a Holocene Thermal Maximum climatology, and/or ignoring the precipitation correction increases this lower bound (SM methods). Modeling ice-free conditions at Camp Century thus provides a strong minimum constraint on the contribution of the GrIS to GMSL during MIS 11.

Discussion

The Camp Century subglacial sediment contains multiple lines of evidence for the deglaciation of northwestern Greenland during the MIS 11 interglacial period (424 to 374 ka). The sorted, stratified upper sediment that contains abundant, well-preserved tundra plant macrofossils and biomarkers (*20*) was transported and deposited by flowing water in an ice-free environment. The coherent distribution of IRSL ages (416 ± 38 ka in 42 aliquots) strongly suggests deposition of the upper sediment in an ice-free environment where the luminescence signal was effectively zeroed by exposure to light at the land surface. Statistically indistinguishable provenance and mineralogy data indicate that sediment in the uppermost sample was derived from the erosion of material similar in composition to that of the lower sample and that both samples originated from the weathering of the Precambrian shield of northern Greenland (*28*). The dominance of garnet over less-durable heavy minerals in the upper sediment suggests additional weathering in an ice-free environment (*27*). The durations we calculate for interglacial exposure at MIS 11, using a combination of ^{26}Al/^{10}Be and luminescence data, are reasonable given other records of MIS 11 duration and are internally consistent at ≤16 kyr (*33*).

The deglaciation of northwestern Greenland during MIS 11 confirms far-field paleoclimate records indicating the GrIS was smaller at this time (Fig. 1B). In Labrador Sea sediment cores, reduced input from specific Greenland bedrock terranes (*7*, *8*) and elevated pollen concentrations [Ocean Drilling Program (ODP) Site 646] (*10*) suggest ice-free and forested conditions in southern Greenland during MIS 11. Although summer sea surface temperatures in the Labrador Sea (*11*, *12*) and Greenland terrestrial summer temperatures (*13*) during MIS 11 were less extreme than other interglacials of

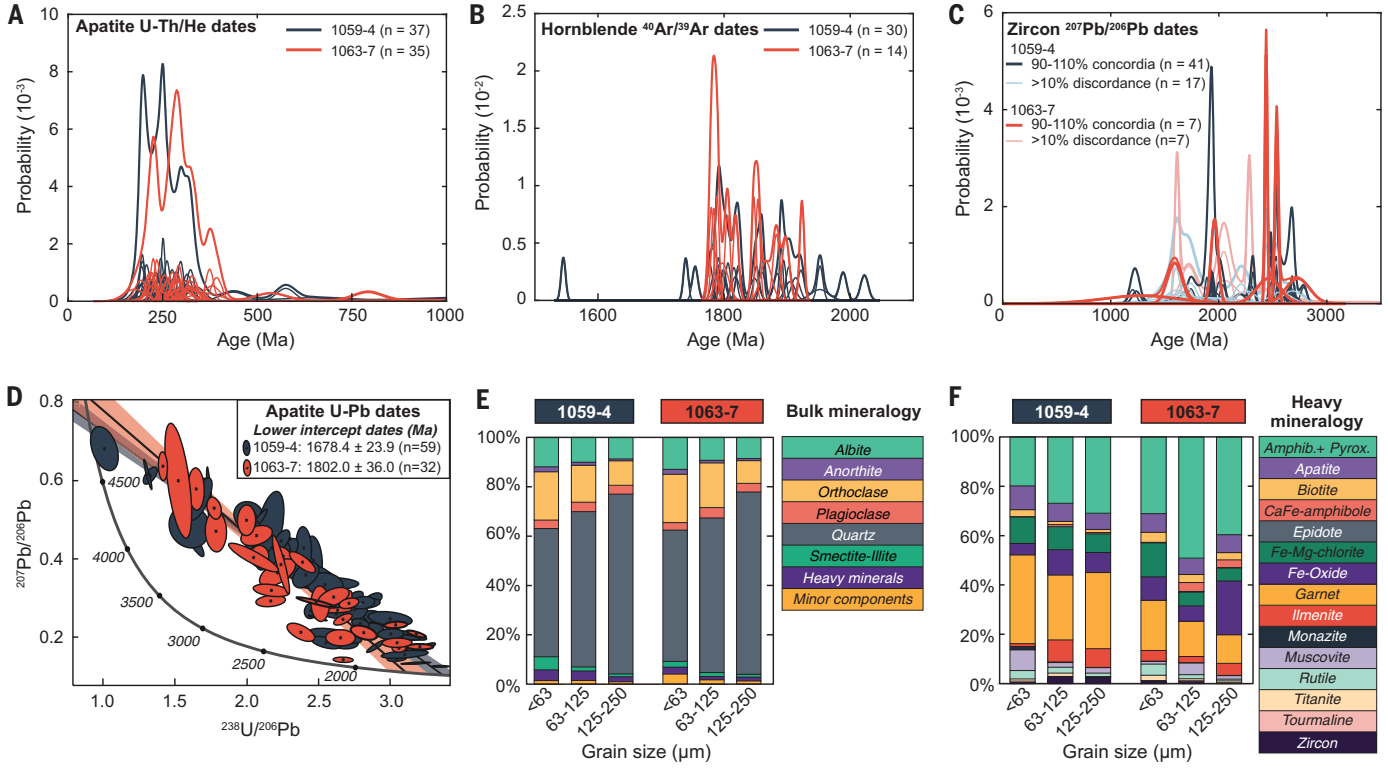

Fig. 5. Detrital geochronometry and mineralogy from the upper (1059-4) and lower (1063-7) sediments. Kernel density functions of (**A**) apatite U-Th/He dates, (**B**) $^{40}Ar/^{39}Ar$ hornblende dates, and (**C**) $^{207}Pb/^{206}Pb$ zircon dates. Thin lines show individual ages and 1σ uncertainty, thick lines show kernel density function. (**D**) Tera-Wasserburg concordia intercept U-Pb dates for apatite. In (A) to (D), *n* refers to the number of dated mineral grains from each sample. (**E**) Bulk and (**F**) heavy mineralogy by percent area determined from automated quantitative mineralogy (data S18).

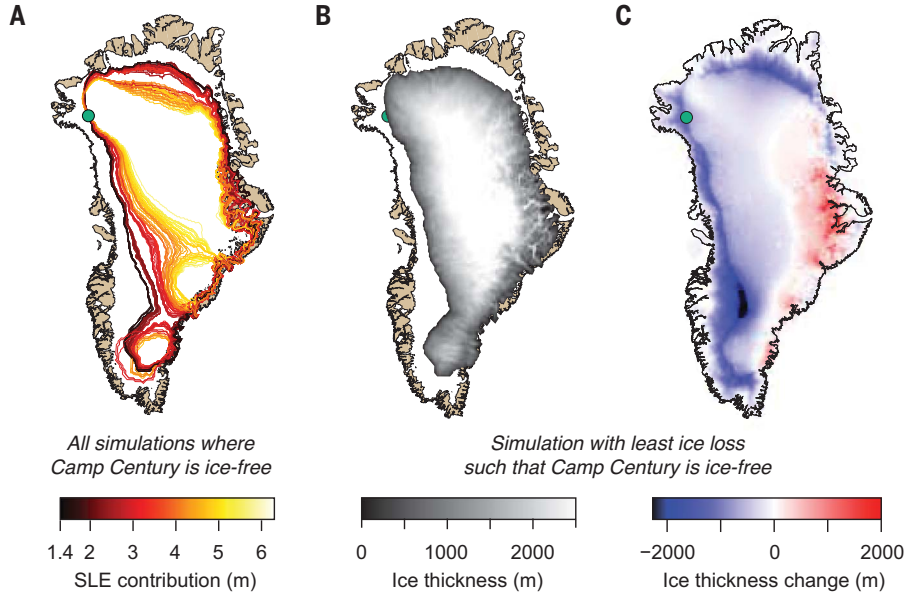

Fig. 6. Ice sheet modeling results that maintain an ice-free Camp Century. (**A**) Ice sheet extent from an ensemble of ice sheet simulations and associated SLE contributions such that Camp Century is ice free, with present ice extent (white) and ice-free areas (tan) shown for comparison. (**B**) Extent and ice thickness and (**C**) ice thickness change relative to modern ice sheet geometry (*32*) of the simulation with the least ice loss such that Camp Century deglaciates. Green circles mark the location of Camp Century.

the past 600 kyr (Fig. 1B), sustained terrestrial summer warmth caused greater retreat of the GrIS during MIS 11 (*11*, *13*). The Labrador Sea proxy studies and ice sheet modeling independently indicate southern GrIS retreat for ~16 kyr before cooling and ice sheet expansion after 390 ka (*7*–*11*, *13*), which is consistent (within uncertainties) with the timing and duration of ice-free conditions in northwest Greenland that we document. Some exposure-burial scenarios modeled from $^{26}Al/^{10}Be$ measurements in GISP2 subglacial bedrock in central Greenland (*17*) are compatible with the deglaciation of southern and northwestern Greenland during MIS 11. However, the persistence of eastern highlands–sourced IRD in the Nordic Sea (*5*) during MIS 11 indicates that at least eastern Greenland remained glaciated. Our ice sheet modeling is consistent with these observations: Simulations that produce ice-free conditions at Camp Century also result in ice retreat in southern Greenland, but nearly all simulations maintain ice cover in the eastern highlands to some degree (Fig. 6A). Isotopic analyses indicate that silt in both GRIP basal ice and GISP2 subglacial till was sourced from the eastern

highlands (*34*); thus, age constraints of GRIP basal ice [950 ± 44 ka (^{10}Be/^{36}Cl) (*14*) or 970 ± 140 ka (δ^{40}Ar/^{38}Ar) (*15*)] further suggest ice cover in the eastern highlands, and possibly central Greenland, during MIS 11.

The deglaciation of northwest Greenland, as demonstrated here, provides important geologic constraints on the GrIS contribution to the MIS 11 GMSL budget, which was +6 to 13 m higher than present (*2*). Previously, the estimated ~4.5 to 6 m SLE contribution from the GrIS during MIS 11 (*2*, *3*) was largely deduced from the total GMSL budget and not based on specific ice sheet sources owing to the scarcity of direct geological constraints from Greenland or Antarctica (*3*). Our ice sheet modeling shows that the GrIS configuration with the least amount of ice loss needed for ice-free conditions at Camp Century produces +1.4 m of SLE from Greenland relative to the present GrIS configuration. However, model-based estimates for GrIS contribution given ice-free conditions at Camp Century include a wide range of results, up to loss of the entire ice sheet and concomitant sea level contribution of ~7 m of SLE (Fig. 6 and fig. S8). Camp Century is located on a local ice dome in a cold area that receives abundant precipitation from Baffin Bay, making this sector of the GrIS resilient to warming. Regardless of how far the GrIS retreated into the interior, ice-free conditions at Camp Century explain ≥1.4 m of SLE contribution from Greenland to the +6 to 13 m GMSL budget of MIS 11 (*2*).

Implications

Our data show substantial retreat of the GrIS during the long, moderately warm MIS 11 interglacial, during which atmospheric carbon dioxide concentrations reached a maximum of 286 parts per million (ppm) (*35*). Northern Hemisphere summer insolation during MIS 11 was not appreciably different from the present, but the duration of peak warmth of MIS 11 was exceptionally long (29 kyr) because of the orbital configuration at the time (*35*–*37*). The extended duration of MIS 11 interglacial warmth resulted in large-scale retreat of the northwestern (this study) and southern GrIS (*7*, *10*, *11*, *13*, *38*). Going forward, the long atmospheric residence time of anthropogenic greenhouse gases will prolong current, human-induced climate warming for many thousands of years. Even under the intermediate Representative Concentration Pathway 4.5, in which atmospheric CO_2 concentrations begin to decline after 2040 CE, atmospheric CO_2 will take ~30 kyr to return to 380 ppm (*39*), which is still ~100 ppm above the concentration reached during MIS 11 (*35*). If moderate warmth for 29 kyr during MIS 11 resulted in substantial ice loss from Greenland, then rapid, prolonged, and considerable anthropogenic Arctic warming (*40*) will likely cause melting of the GrIS, raise sea level, and trigger additional climate feedbacks in the coming centuries (*41*–*43*).

REFERENCES AND NOTES

1. H. Elderfield *et al*., *Science* **337**, 704–709 (2012).
2. M. E. Raymo, J. X. Mitrovica, *Nature* **483**, 453–456 (2012).
3. A. Dutton *et al*., *Science* **349**, aaa4019 (2015).
4. B. Dyer *et al*., *Proc. Natl. Acad. Sci. U.S.A.* **118**, e2026839118 (2021).
5. E. Jansen, T. Fronval, F. Rack, J. E. T. Channell, *Paleoceanography* **15**, 709–721 (2000).
6. P. R. Bierman, J. D. Shakun, L. B. Corbett, S. R. Zimmerman, D. H. Rood, *Nature* **540**, 256–260 (2016).
7. A. V. Reyes *et al*., *Nature* **510**, 525–528 (2014).
8. R. G. Hatfield *et al*., *Earth Planet. Sci. Lett.* **454**, 225–236 (2016).
9. E. J. Colville *et al*., *Science* **333**, 620–623 (2011).
10. A. de Vernal, C. Hillaire-Marcel, *Science* **320**, 1622–1625 (2008).
11. N. Irvalı *et al*., *Proc. Natl. Acad. Sci. U.S.A.* **117**, 190–195 (2020).
12. N. Irvalı *et al*., *Quat. Sci. Rev.* **150**, 184–199 (2016).
13. A. A. Cluett, E. K. Thomas, *Proc. Natl. Acad. Sci. U.S.A.* **118**, e2022916118 (2021).
14. E. Willerslev *et al*., *Science* **317**, 111–114 (2007).
15. A. M. Yau, M. L. Bender, T. Blunier, J. Jouzel, *Earth Planet. Sci. Lett.* **451**, 1–9 (2016).
16. M. L. Bender, E. Burgess, R. B. Alley, B. Barnett, G. D. Clow, *Earth Planet. Sci. Lett.* **299**, 466–473 (2010).
17. J. M. Schaefer *et al*., *Nature* **540**, 252–255 (2016).
18. NEEM community members, *Nature* **493**, 489–494 (2013).
19. T. Goossens *et al*., *Cryosphere* **10**, 553–567 (2016).
20. A. J. Christ *et al*., *Proc. Natl. Acad. Sci. U.S.A.* **118**, e2021442118 (2021).
21. B. L. Hansen, C. C. Langway Jr., *Antarct. J. US.* **1**, 207–208 (1966).
22. D. M. Harwood, *Arctic* **39**, 304–308 (1986).
23. B. Li, S.-H. Li, *Quat. Geochronol.* **6**, 468–479 (2011).
24. M. Lamothe, M. Auclair, C. Hamzaoui, S. Huot, *Radiat. Meas.* **37**, 493–498 (2003).
25. J. P. Buylaert *et al*., *Geochronometria* **38**, 432–440 (2011).
26. L. B. Corbett *et al*., *Geophys. Res. Lett.* **44**, 1350–1359 (2017).
27. J. E. Saylor, K. E. Sundell, *Geosphere* **12**, 203–220 (2016).
28. A. P. Nutman, P. R. Dawes, F. Kalsbeek, M. A. Hamilton, *Precambrian Res.* **161**, 419–451 (2008).
29. K. Thrane, C. Knudsen, N. Keulen, E. Burden, *Danmarks og Grønlands Geol. Undersøgelse Rapp.* **2010/2012** (2010).
30. C. Buizert *et al*., *Science* **345**, 1177–1180 (2014).
31. C. Buizert *et al*., *Geophys. Res. Lett.* **45**, 1905–1914 (2018).
32. M. Morlighem *et al*., *Geophys. Res. Lett.* **44**, 11051–11061 (2017).
33. M. J. Wilson, *Clay Miner.* **39**, 233–266 (2004).
34. D. Weis, D. Demaiffe, R. Souchez, A. J. Gow, D. A. Meese, *Earth Planet. Sci. Lett.* **150**, 161–169 (1997).
35. Past Interglacials Working Group of PAGES, *Rev. Geophys.* **54**, 162–219 (2016).
36. A. V. Sundal *et al*., *Nature* **469**, 521–524 (2011).
37. P. C. Tzedakis, D. A. Hodell, C. Nehrbass-ahles, T. Mitsui, E. W. Wolff, *Quat. Sci. Rev.* **284**, 107493 (2022).
38. A. Robinson, J. Alvarez-Solas, R. Calov, A. Ganopolski, M. Montoya, *Nat. Commun.* **8**, 16008 (2017).
39. J. E. Tierney *et al*., *Science* **370**, eaay3701 (2020).
40. M. Rantanen *et al*., *Commun. Earth Environ.* **3**, 168 (2022).
41. A. Aschwanden *et al*., *Sci. Adv.* **5**, eaav9396 (2019).
42. M. Zeitz, R. Reese, J. Beckmann, U. Krebs-Kanzow, R. Winkelmann, *Cryosphere* **15**, 5739–5764 (2021).
43. J. E. Box *et al*., *Nat. Clim. Chang.* **12**, 808–813 (2022).
44. J. Fountain, T. M. Usselman, J. Wooden, C. C. Langway Jr., *J. Glaciol.* **27**, 193–197 (1981).

ACKNOWLEDGMENTS

We thank M. Kirk and I. Koldtoft for sample shipping coordination, M. Alaei and H. Vesturklett for mineralogy and U/Pb sample preparation, S. N. Malkki for mineralogical analyses, B. D. Heredia for laser ablation inductively coupled plasma mass spectrometry analysis, and S. Huot for assistance with the fading correction of MET pIRSL ages. **Funding:** This work was supported by NSF ANS 2114629 (A.J.C., P.R.B., and N.P.); NSF-ANS 2114630 (T.M.R.); Geocenter Denmark Grant GC-3-2019 (P.C.K.); NSF EAR-IF 1652274 and NSF ANS 2114632 (E.K.T.); NSF EAR-LTS 1735492 (J.C.F.); and NSF ANS 2114631 (E.J.S.). Prepared in part by LLNL under contract DE-AC52-07NA27344; LLNL-JRNL-837984 (A.J.H.). **Author contributions:** Conceptualization: A.J.C., T.M.R., and P.R.B. Methodology: A.J.C., T.M.R., B.A.K., P.C.K., T.B.T., N.K., J.C.F., S.R.H., J.-L.T., and P.-H.B. Investigation: A.J.C., T.M.R., B.A.K., P.C.K., T.B.T., N.K., J.C.F., S.R.H., J.-L.T., and P.-H.B. Visualization: A.J.C., T.M.R., B.A.K., P.C.K., T.B.T., N.K., J.C.F., and S.R.H. Funding acquisition: P.R.B., A.J.C., N.P., T.M.R., M.W.C., E.J.S., E.K.T., and J.P.S. Writing – original draft: A.J.C., T.M.R., P.R.B., B.A.K., P.C.K., T.B.T., N.K., J.C.F., S.R.H., J.-L.T., and P.-H.B. Writing – review & editing: J.P.S., M.W.C., L.B.C., D.D.-J., D.P.D., A.J.H., N.P., D.M.P., E.J.S., and E.K.T. **Competing interests:** The authors declare no competing interests. **Data and materials availability:** All data are available in the supplementary materials. The code used for the ^{26}Al/^{10}Be exposure-burial modeling is available here: https://github.com/drewchrist-geo/Camp_Century_complex_26Al10Be_modelling.git.

SUPPLEMENTARY MATERIALS

science.org/doi/10.1126/science.ade4248
Materials and Methods
Figs. S1 to S9
References (*45*–*80*)
Data S1 to S19

Submitted 2 September 2022; accepted 21 June 2023
10.1126/science.ade4248